β5, but the efficiency with which they inhibited binding to β5 was much lower than that of β1; at a concentration of 10 μM, the compounds almost completely inhibited binding of belactosin A to β1, whereas binding to β5 was still detectable at 100 μM. These results suggest that the region in which the RID-F compounds bind β5 is proximal to the CT-L active site and partially overlaps the binding region of belactosin A. The concentration (10 μM) of the RID-F derivatives required to inhibit binding of belactosin to β1 (PGPH activity) was much higher than the K_i (submicromolar levels) determined from kinetic analyses (Fig. 1A). There are several potential explanations for this difference: (i) the affinity of biotin-labeled belactosin A was higher than that of the substrate used for kinetic analyses, or (ii) the reversible inhibitor RID-F derivatives are eventually replaced by the covalent inhibitor, belactosin. MG132, which was used as a positive control for proteasomal protease inhibition, prevented biotin-belactosin A from forming covalent linkages to all subunits. RID-F-S*110 (**30**) showed little effect on belactosin binding (Fig. 2C), which was consistent with the result indicating that this compound has minimal inhibitory potency against proteasomal activity (Table 5). The possible mechanism by which RID-F derivatives prevent the binding of belactosin to the β2 subunit (T-L activity) remains to be studied.

2.5. Cytotoxicity

We also evaluated the effect of the RID-F derivatives on proliferation of two human cell lines, human embryonic kidney 293 cells (HEK293, ER-negative) and HL-60 cells (ER-positive). Cells were treated with different concentrations of each compound for 48 h, after which the number of live cells was determined using a 3-(4,5-dimethylthiazol-2-yl)-2,5-diphenyltetrazolium bromide (MTT) assay. The CyT_{50}, defined as the concentration required for 50% inhibition of cell proliferation (see Experimental section), was determined for each compound, and the results are summarized in Tables 2–5. The compounds with poor inhibitory potency (IC_{50} > 10 μM) against CT-L activity *in vitro* were not cytotoxic, with the exception of RID-F-S*22 (**19**), which significantly inhibited CT-L activity but was inexplicably noncytotoxic. Most of the cytotoxic compounds showed similar toxicity to both cell types, although some compounds (RID-F-S*12 (**11**), RID-F-S*11 (**12**) and RID-F-S*6 (**28**)) were more toxic to HL60 than HEK293 cells, and two compounds (RID-F-S*5 (**23**) and RID-F-S*103 (**29**)) were more toxic to HEK293 cells.

Is the cytotoxicity of RID-F derivatives attributable to their inhibition of proteasome activity? To address this question, we selected compounds that inhibited at least two of the three proteasome protease activities. The IC_{50} values of these compounds were plotted against the CyT_{50} values determined using HEK293 cells to estimate the correlation between proteasome inhibition and cytotoxicity (Fig. 3A). The correlation coefficients were 0.51 for CT-L activity and 0.48 for PGPH activity (Fig. 3B) but only 0.02 for T-L activity (Fig. 3C). Thus, it is very likely that the cytotoxicity of the RID-F derivatives is caused by their inhibition of proteasome CT-L and PGPH activities, whereas the inhibition of T-L activity is not associated with cytotoxicity. It is not known whether inhibition of either CT-L or PGPH activity alone is sufficient to cause cytotoxicity or if inhibition of both activities is required. Genetic studies have suggested that CT-L activity is essential for proteasome function, because mutational loss of CT-L activity causes a significant reduction in the degradation of proteasomal substrates [42,43]. Taken together, these data suggest that the inhibition of CT-L activity by RID-F derivatives may be linked to cell death. The CyT_{50} values of the RID-F derivatives were generally one order of magnitude higher than the corresponding IC_{50} values; restricted diffusion of the derivatives through the cell membrane may be responsible for this difference.

We next investigated the ability of the RID-F derivatives to inhibit proteasome function in cultured cells. HeLa cells were incubated with RID-F (**6**), RID-F-S*4 (**25**), or RID-F-S*110 (**30**), and the accumulation of ubiquitinated proteins was examined by Western blotting. A significant accumulation of multiple bands of high-molecular-weight ubiquitinated proteins was observed in

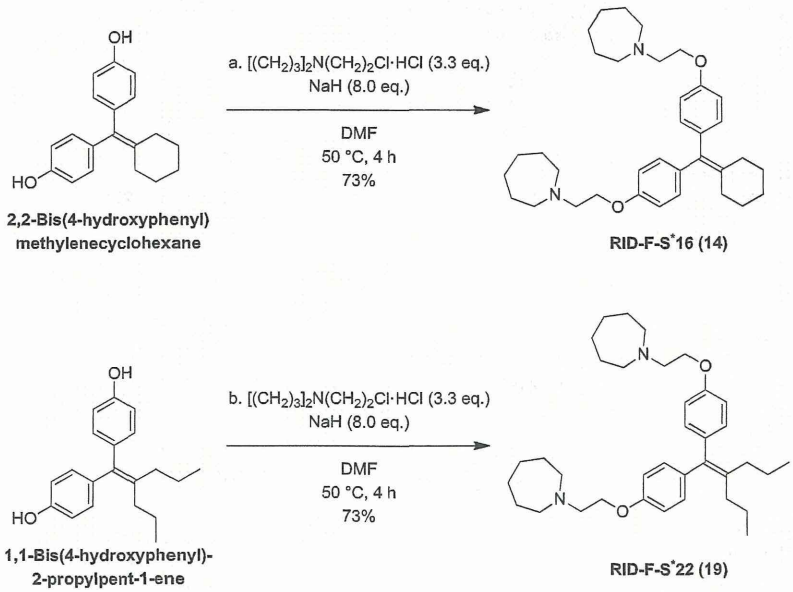

Reagents and conditions: (a) $[(CH_2)_3]_2N(CH_2)_2Cl{\cdot}HCl$ (3.3 eq.), NaH (8.0 eq.), DMF, 50 °C, 4 h, 73%; (b) $[(CH_2)_3]_2N(CH_2)_2Cl{\cdot}HCl$ (3.3 eq.), NaH (8.0 eq.), DMF, 50 °C, 4 h, 73%.

Scheme 6. Synthesis of RID-F-S*16 (**14**) and RID-F-S*22 (**19**) from 2,2-bis(4-hydroxyphenyl)methylenecyclohexane and 1,1-bis(4-hydroxyphenyl)-2-propylpent-1-ene.

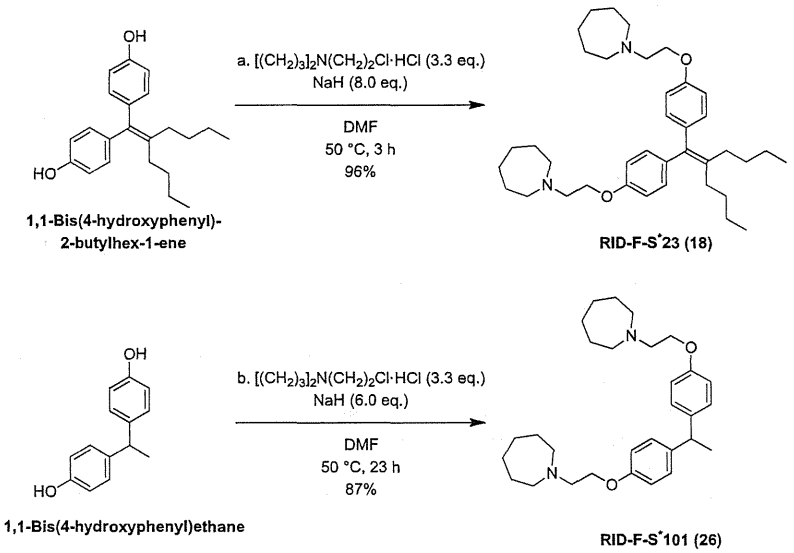

Reagents and conditions: (a) $[(CH_2)_3]_2N(CH_2)_2Cl{\cdot}HCl$ (3.3 eq.), NaH (8.0 eq.), DMF, 50 °C, 3 h, 96%; (b) $[(CH_2)_3]_2N(CH_2)_2Cl{\cdot}HCl$ (3.3 eq.), NaH (6.0 eq.), DMF, 50 °C, 23 h, 87%.

Scheme 7. Synthesis of RID-F-S*23 (**18**) and RID-F-S*101 (**26**) from 1,1-bis(4-hydroxyphenyl)-2-butylhex-1-ene and 1,1-bis(4-hydroxyphenyl)ethane.

cells treated with RID-F (**6**) and RID-F-S*4 (**25**) (Fig. 4, lanes 3 and 4). The accumulation of such proteins was minimal in cells treated with RID-F-S*110 (**30**), a compound that showed very low inhibition potency (Table 5). Accumulation of ubiquitinated proteins was also observed in lysates of cells treated with the known proteasome inhibitor, MG132 (Fig. 4, lane 2). These data indicate that RID-F derivatives inhibit proteasome activities in cells.

Abnormal accumulation of proteins resulting from the inhibition of proteasome activity has antiproliferative effects on cells, including induction of apoptosis. Therefore, we examined

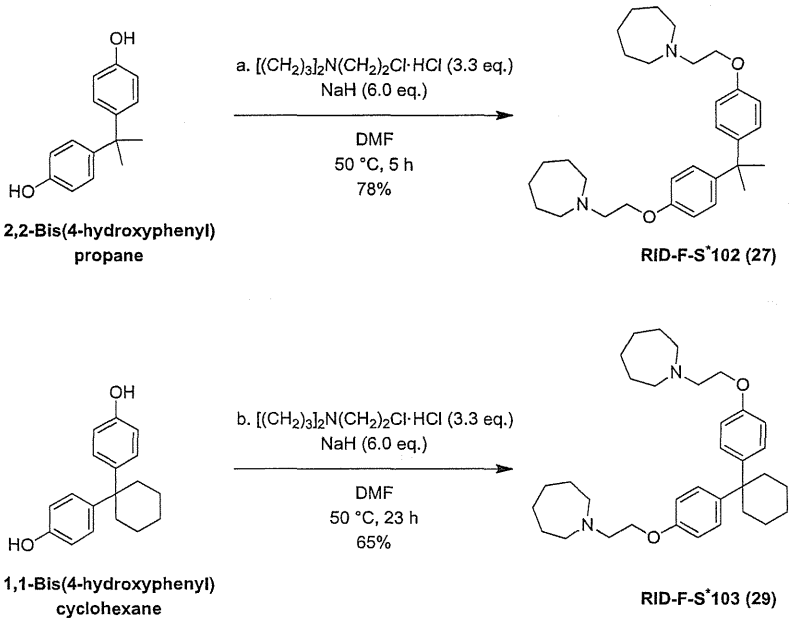

Reagents and conditions: (a) $[(CH_2)_3]_2N(CH_2)_2Cl{\cdot}HCl$ (3.3 eq.), NaH (6.0 eq.), DMF, 50 °C, 5 h, 78%; (b) $[(CH_2)_3]_2N(CH_2)_2Cl{\cdot}HCl$ (3.3 eq.), NaH (6.0 eq.), DMF, 50 °C, 23 h, 65%.

Scheme 8. Synthesis of RID-F-S*102 (**27**) and RID-F-S*103 (**29**) from 2,2-bis(4-hydroxyphenyl)propane and 1,1-bis(4-hydroxyphenyl)cyclohexane.

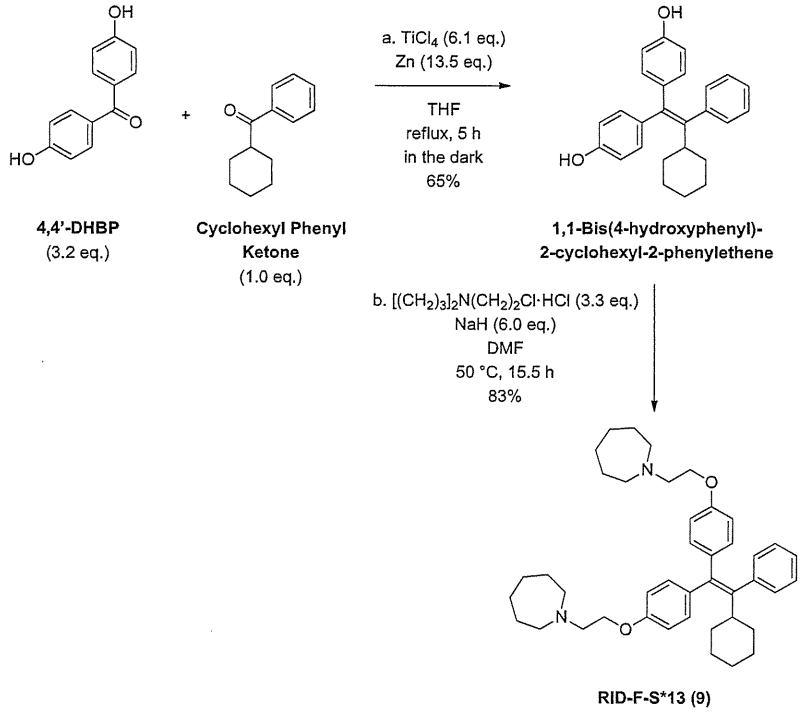

Reagents and conditions: (a) $TiCl_4$ (6.1 eq.), Zn (13.5 eq.), THF, reflux, 5 h in the dark, 65%; (b) $[(CH_2)_3]_2N(CH_2)_2Cl{\cdot}HCl$ (3.3 eq.), NaH (6.0 eq.), DMF, 50 °C, 15.5 h, 83%.

Scheme 9. Synthesis of RID-F-S*13 (**9**) from 4,4′-dihydroxybenzophenone (4,4′-DHBP) and cyclohexyl phenyl ketone.

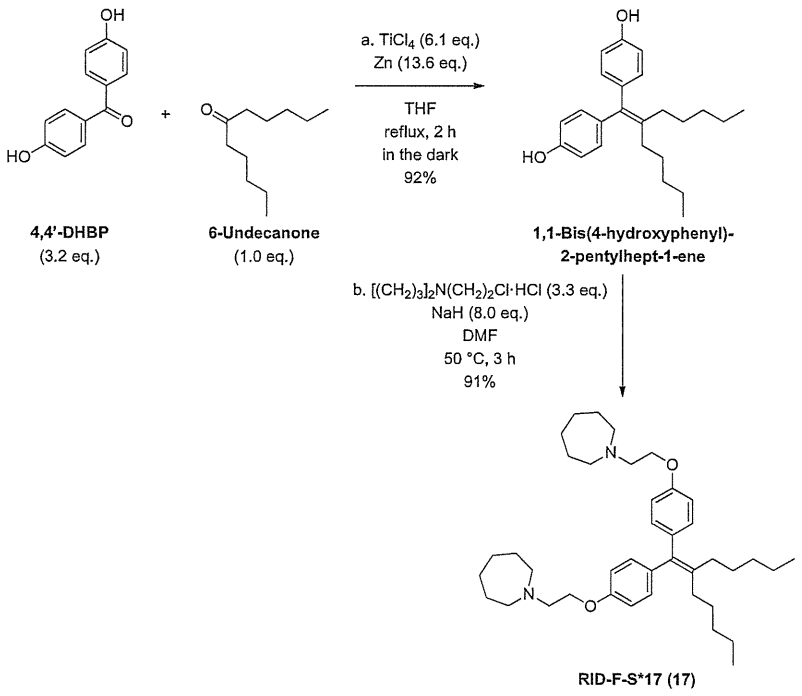

Reagents and conditions: (a) $TiCl_4$ (6.1 eq.), Zn (13.6 eq.), THF, reflux, 2 h in the dark, 92%; (b) $[(CH_2)_3]_2N(CH_2)_2Cl{\cdot}HCl$ (3.3 eq.), NaH (8.0 eq.), DMF, 50 °C, 3 h, 91%.

Scheme 10. Synthesis of RID-F-S*17 (**17**) from 4,4′-dihydroxybenzophenone (4,4′-DHBP) and 6-undecanone.

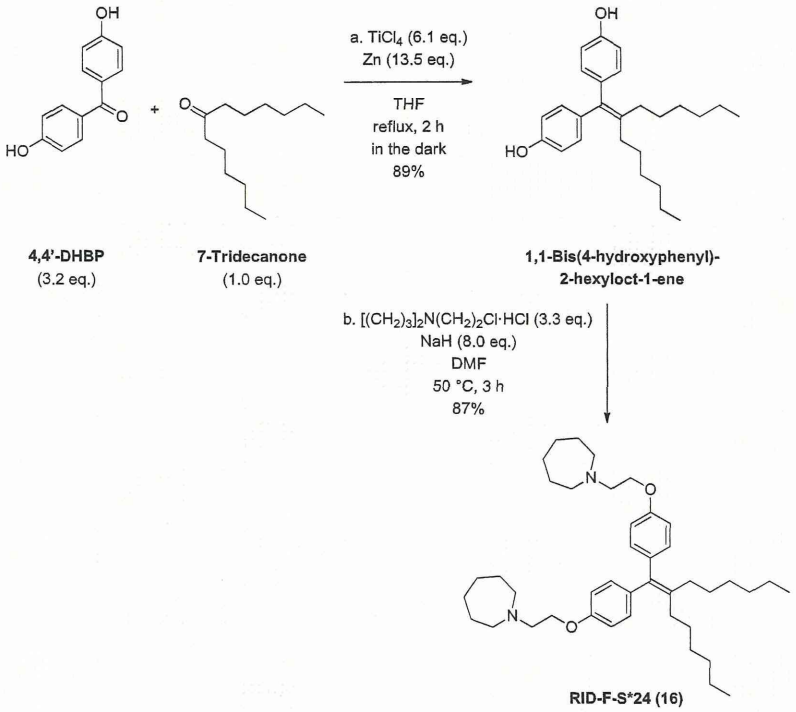

Reagents and conditions: (a) $TiCl_4$ (6.1 eq.), Zn (13.5 eq.), THF, reflux, 2 h in the dark, 89%; (b) $[(CH_2)_3]_2N(CH_2)_2Cl{\cdot}HCl$ (3.3 eq.), NaH (8.0 eq.), DMF, 50 °C, 3 h, 87%.

Scheme 11. Synthesis of RID-F-S*24 (**16**) from 4,4′-dihydroxybenzophenone (4,4′-DHBP) and 7-tridecanone.

Table 2
Inhibition of human 20S proteasome activity by RID-F derivatives and their cytotoxic effect on human cells (HEK293 and HL-60).

Compound number		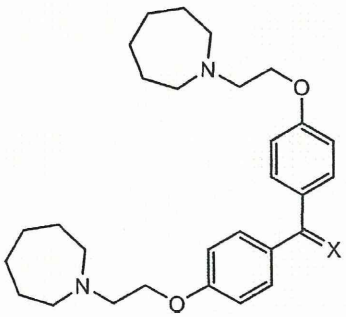	IC_{50} (μM)[a]			HEK293	CyT_{50} (μM)[b]
			CT-L	T-L	PGPH		HL-60
9	RID-F-S*13	X = C(*c*-Hex)Ph	>10	>10	0.35 ± 0.02	>30	>30
10	RID-F-S*14	X = CPh_2	1.18 ± 0.07	>10	0.37 ± 0.06	23.2 ± 1.1	>30
11	RID-F-S*12	X = C(*n*-C_3H_7)Ph	1.37 ± 0.27	0.28 ± 0.04	1.05 ± 0.46	26.8 ± 1.0	4.30 ± 0.55
6	RID-F	X = C(C_2H_5)Ph	0.64 ± 0.14	0.34 ± 0.12	0.43 ± 0.08	4.38 ± 0.79	3.42 ± 0.33
12	RID-F-S*11	X = C(CH_3)Ph	0.90 ± 0.10	0.36 ± 0.17	0.87 ± 0.04	18.9 ± 1.2	6.87 ± 1.47
13	RID-F-S*1	X = CHPh	0.58 ± 0.05	0.69 ± 0.54	0.37 ± 0.19	6.06 ± 0.45	9.73 ± 0.62
14	RID-F-S*16	X = 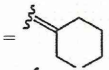	2.19 ± 0.25	2.18 ± 2.03	0.89 ± 0.09	12.5 ± 0.3	11.7 ± 0.4
15	RID-F-S*15	X = 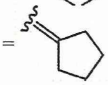	2.70 ± 0.10	1.11 ± 0.08	1.67 ± 0.15	26.2 ± 1.9	20.1 ± 0.6

[a] IC_{50} values denote concentrations of the compounds required for 50% inhibition of the activities (see "Experimental section"). CT-L, chymotrypsin-like activity; T-L, trypsin-like activity; PGPH, peptidylglutamyl peptide hydrolase activity. NT, not tested.
[b] CyT_{50} values denote concentration of the compounds required for 50% inhibition of the cell proliferation (see "Experimental section"). Values are means of triplicate.

Table 3
Inhibition of 20S proteasome activity by RID-F derivatives substituted with aliphatic chains at the center sp^2 carbon (X) and their cytotoxic effect on human cells.

Compound number		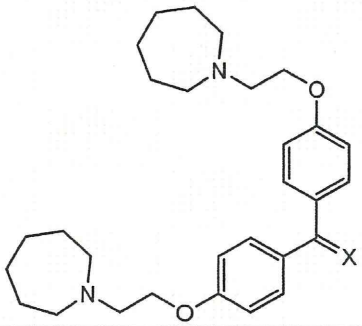	IC_{50} (μM)[a]			HEK293	CyT_{50} (μM)[b]
			CT-L	T-L	PGPH		HL-60
16	RID-F-S*24	X = C(*n*-$C_6H_{13})_2$	>10	>10	>10	>30	>30
17	RID-F-S*17	X = C(*n*-$C_5H_{11})_2$	>10	>10	>10	14.5 ± 3.9	>30
18	RID-F-S*23	X = C(*n*-$C_4H_9)_2$	>10	>10	>10	>30	25.3 ± 0.6
19	RID-F-S*22	X = C(*n*-$C_3H_7)_2$	3.38 ± 0.42	>10	2.51 ± 0.44	>30	>30
20	RID-F-S*10	X = $C(C_2H_5)_2$	1.57 ± 0.70	0.96 ± 0.18	0.84 ± 0.12	6.02 ± 0.14	8.87 ± 1.13
21	RID-F-S*9	X = $C(CH_3)_2$	1.66 ± 0.12	>10	1.20 ± 0.19	11.1 ± 0.5	10.7 ± 1.6
22	RID-F-S*2	X = $CH(C_2H_5)$	1.46 ± 0.14	1.61 ± 0.47	1.03 ± 0.10	26.7 ± 0.8	22.6 ± 0.3
23	RID-F-S*5	X = O	1.65 ± 0.21	8.59 ± 1.75	1.56 ± 0.08	13.9 ± 1.4	>30
24	RID-F-S*3	X = CH_2	1.04 ± 0.22	0.88 ± 0.45	0.91 ± 0.04	9.80 ± 5.53	10.7 ± 0.5

[a] IC_{50} values denote concentrations of the compounds required for 50% inhibition of the activities (see "Experimental section"). CT-L, chymotrypsin-like activity; T-L, trypsin-like activity; PGPH, peptidylglutamyl peptide hydrolase activity. NT, not tested.
[b] CyT_{50} values denote concentration of the compounds required for 50% inhibition of the cell proliferation (see "Experimental section"). Values are means of triplicate.

whether the observed cytotoxicity of RID-F derivatives was due to apoptosis. MG132, a representative proteasome inhibitor that binds all three subunits, was used as a control compound. Cleavage of poly(ADP-ribose) polymerase (PARP) is one of the hallmarks of apoptosis. RID-F (**6**) (Fig. 5A) and RID-F-S*4 (**25**) (Fig. 5B) caused PARP cleavage in a dose-dependent manner, but PARP cleavage was almost undetectable in cells treated with RID-F-S*110 (**30**) (Fig. 5C), which was consistent with the very low inhibition of proteasome activities demonstrated by this compound (Table 5). RID-F-induced apoptosis was confirmed by cleavage of caspase 3 (Supplementary Fig. S1) and an increase in the proportion of cells in the sub-G1 fraction as determined by flow cytometry (Supplementary Fig. S2). These results indicate that the cytotoxicity of RID-F derivatives can be attributed at least in part to apoptosis.

2.6. Three-dimensional modeling of RID-F derivatives bound to the yeast proteasome subunit PRE3

How do RID-F derivatives bind the proteasome to exhibit their inhibitory effect? Docking studies were conducted to attempt to answer this question. To date, no reports of the experimental determination of the 3D structure of the human 20S proteasome have been published. However, several 3D structures of the yeast proteasome have been reported. The molecular structure of the ligand-binding pockets of the yeast and mammalian proteasomes is

Table 4
Inhibition of 20S proteasome activity by RID-F derivatives with aliphatic side structures at the center sp^3 carbon (X) and their cytotoxic effect on human cells.

Compound number		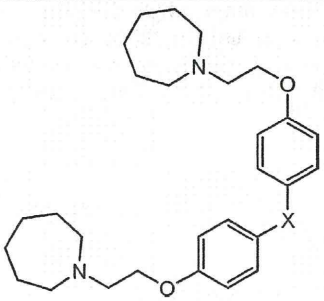	IC_{50} (μM)[a]			HEK293	CyT_{50} (μM)[b]
			CT-L	T-L	PGPH		HL-60
25	RID-F-S*4	X = CH_2	0.67 ± 0.04	0.99 ± 0.21	0.63 ± 0.15	10.9 ± 0.6	14.5 ± 0.3
26	RID-F-S*101	X = $CH(CH_3)$	0.80 ± 0.02	>10	0.79 ± 0.02	8.12 ± 0.14	21.4 ± 0.6
27	RID-F-S*102	X = $C(CH_3)_2$	0.75 ± 0.01	1.87 ± 0.83	0.77 ± 0.01	7.61 ± 0.05	17.6 ± 1.8
28	RID-F-S*6	X = $C(CH_3)OH$	1.66 ± 0.11	2.95 ± 0.40	1.35 ± 0.05	22.7 ± 6.3	7.06 ± 0.48
29	RID-F-S*103	X = 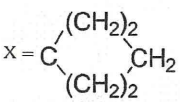	1.94 ± 0.09	0.20 ± 0.20	1.08 ± 0.16	17.5 ± 0.3	>30

[a] IC_{50} values denote concentrations of the compounds required for 50% inhibition of the activities (see "Experimental section"). CT-L, chymotrypsin-like activity; T-L, trypsin-like activity; PGPH, peptidylglutamyl peptide hydrolase activity. NT, not tested.
[b] CyT_{50} values denote concentration of the compounds required for 50% inhibition of the cell proliferation (see "Experimental section"). Values are means of triplicate.

Table 5
Inhibition of 20S proteasome activity by a RID-F derivative missing one of the two homopiperidine rings and its cytotoxic effect on human cells.

Compound number			IC_{50} (μM)[a]			CyT_{50} (μM)[b] HEK293	HL-60
			CT-L	T-L	PGPH		
30	RID-F-S*110	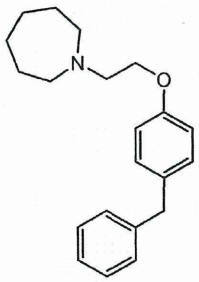	>10	>10	>10	27.0 ± 3.7	>30

[a] IC_{50} values denote concentrations of the compounds required for 50% inhibition of the activities (see "Experimental section"). CT-L, chymotrypsin-like activity; T-L, trypsin-like activity; PGPH, peptidylglutamyl peptide hydrolase activity. NT, not tested.
[b] CyT_{50} values denote concentration of the compounds required for 50% inhibition of the cell proliferation (see "Experimental section"). Values are means of triplicate.

highly conserved [44,45]. Moreover, RID-F also inhibited yeast proteasome CT-L activity, with an IC_{50} of 1.8 μM, which was similar to that (IC_{50} 0.65 μM) determined for the human 20S proteasome (Table 1). These results suggest that the binding modes of the RID-F derivatives to the yeast and human proteasomes are similar. Therefore, we used the yeast proteasome structure for docking simulations of RID-F derivatives.

We used structure data of the yeast 20S proteasome complexed with fellutamide B (PDB ID: 3d29) for docking simulations. The PRE3 subunit (chain N) is the yeast counterpart of the human 20S proteasome β1 subunit, which exhibits PGPH activity. This subunit is sandwiched between the PUP1 subunit (chain H) and the PRE4 subunit (chain M) in the β ring, and the ligand-binding cleft of the PRE3 subunit is formed by these three subunits. Therefore, the trimer structure of chains H, N, and M was used for docking simulations. Using Molecular Operating Environment software, version 2010.10 (MOE 2010.10, Chemical Computing Group Inc.), the energy-minimized trimer structure with hydrogen atoms was prepared with the default parameters. The possible ligand-binding site in the trimer structure was detected using the Site Finder application of MOE 2010.10, with the Connection Distance parameter set to 1.9 Å. Docking simulations involving the RID-F derivatives and the trimer structure were then carried out using ASEDock [46], with the standard procedure.

The best-fitted inhibitor positions near in the active center Thr1 residue suggested that compounds **6** (RID-F), **9**, **10**, **11**, **12**, **13**, **14**, **15**, **20**, **22**, and **23** (but not compounds **19**, **21**, **24** and **25** (RID-F-S*4)) have a similar binding mode. Fig. 6 (A and B) shows the highest-ranked binding mode of docked RID-F (**6**), illustrating molecular interactions between RID-F and the PRE3 catalytic site. One of the important points in the interaction between RID-F and the proteasome appears to be the contact area of the S1 pocket around Thr1. The vinyl benzene group in the side structure of RID-F is in contact with the S1 pocket and has a CH–π interaction with Thr21. The contacted residues delimit the binding pocket size at 120 $Å^3$, in which Thr1 is located at the bottom. These docking simulation results are in agreement with the experimental evidence indicating that the size of the RID-F derivative side structure is critical for binding to the catalytic site.

As the exceptional case, docking simulations involving compounds **19**, **21**, **24**, and **25** (RID-F-S*4) showed one homopiperidine ring contacting the S1 pocket. Their side structures at the X position were either too large or too small. RID-F-S*4 (**25**), which has a high inhibition potency despite the absence of a side structure, binds in a different fashion, as shown in Fig. 6. One terminal homopiperidine moiety in RID-F-S*4 (**25**) enters into the binding cleft in the S1 pocket, as opposed to the vinyl benzene group of RID-F (**6**). These results imply that RID-F derivatives have two modes of binding to the catalytic sites. Interestingly, the results of the docking simulations involving compounds **19**, **21**, **24**, and **25** (RID-F-S*4) suggest that they access the active site in a manner different from that of compound **6** (RID-F), which contacts the active site via the vinyl

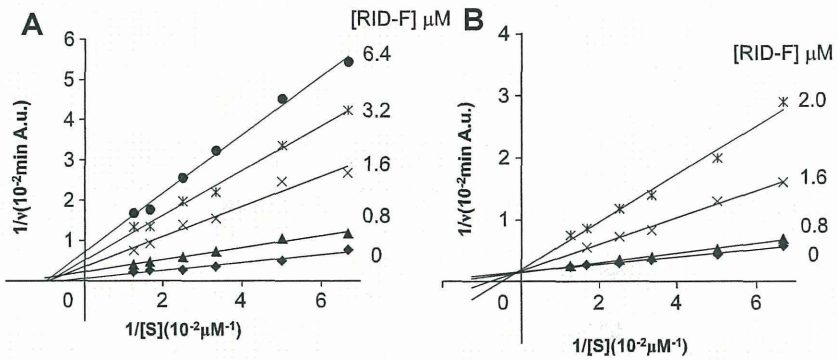

Fig. 1. Lineweaver–Burk plots of the inhibition of proteasomal CT-L and PGPH activities by RID-F. A, CT-L activity. B, PGPH activity. CT-L and PGPH activities were determined using a fluorometric assay as described in the Experimental section, varying the concentrations of substrate and RID-F as indicated. A.U. represents arbitrary units of fluorescence.

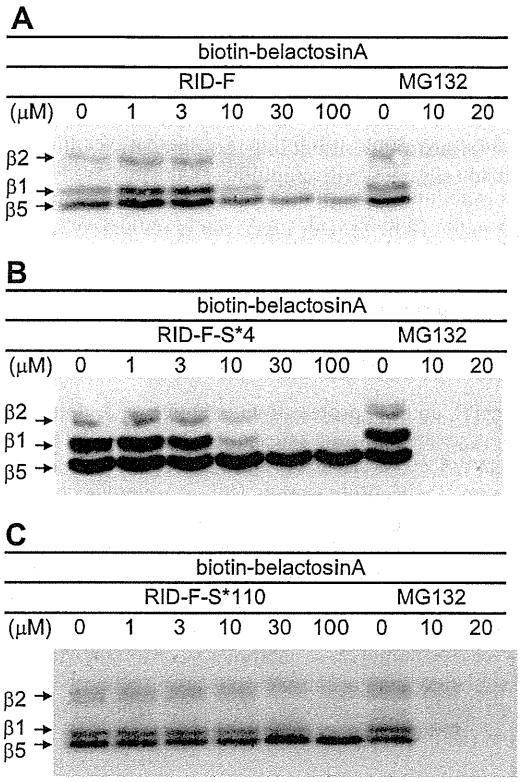

Fig. 2. Inhibition by RID-F derivatives of biotin-labeled belactosin A binding to the proteasome. As described in the Experimental section, human 20S proteasomes were treated with biotin-belactosin A in the presence of RID-F (**6**) (A), RID-F-S*4 (**25**) (B), or RID-F-S*110 (**30**) (C), and biotin-labeled subunits (β1 for T-L activity, β2 for PGPH activity, and β5 for CT-L activity) were then detected. MG132 was used as a control.

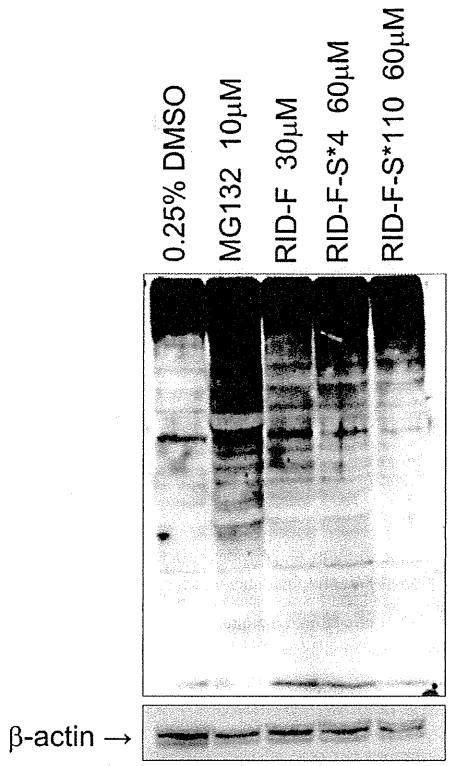

Fig. 4. Accumulation of ubiquitinated proteins induced by RID-F (**6**), RID-F-S*4 (**25**), and RID-F-S*110 (**30**). HeLa cells were treated with 0.25% DMSO (control), MG132 (10 μM), RID-F (30 μM), RID-F-S*4 (60 μM), or RID-F-S*110 (60 μM) for 24 h. Whole cell lysates were immunoblotted with anti-ubiquitin antibody. β-Actin was used as a loading control.

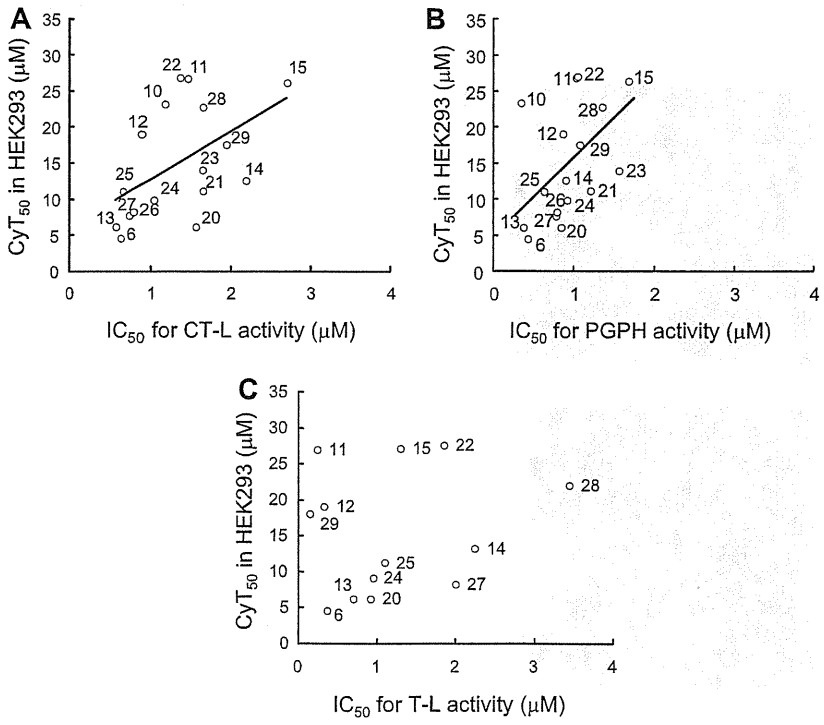

Fig. 3. Correlation between cytotoxicity (CyT_{50}) to HEK293 cells and inhibitory potency against the CT-L and PGPH activities of the human 20S proteasome. A, CyT_{50} versus IC_{50} for CT-L activity. B, CyT_{50} versus IC_{50} for PGPH activity. C, CyT_{50} versus IC_{50} for T-L activity. Numbers in the plots correspond to the compound numbers listed in Tables 2–4.

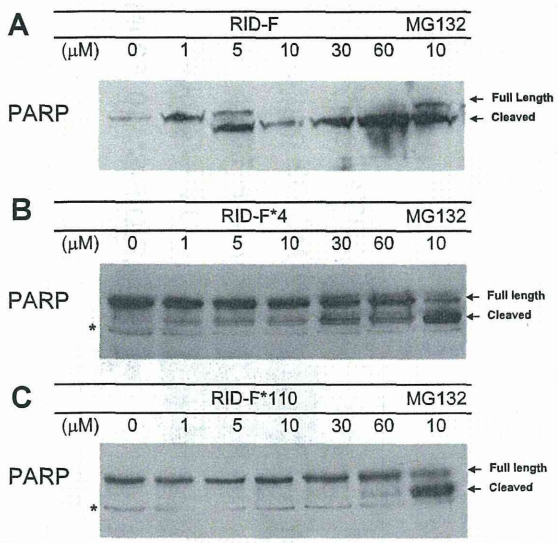

Fig. 5. Apoptosis induced by RID-F derivatives. HeLa cells were incubated with the compounds at indicated concentrations, after which cleavage of PARP was determined by Western blotting (see Experimental section). A, RID-F (**6**); B, RID-F-S*4 (**25**); C, RID-F-S*110 (**30**). MG132, a proteasome inhibitor that induces PARP cleavage, which is a hallmark of apoptosis, was used as a control. * = nonspecific bands.

benzene at the X position. As illustrated in Fig. 6 (C and D) for RID-F-S*4 (**25**) as a representative, these RID-F derivatives may interact with the S1 pocket via one of the homopiperidine rings. The side structures at the X positions in these four compounds were too large or too small in comparison with the optimal size of vinyl benzene. Thus, it appears that not only the presence of two homopiperidine rings but also the relationship between the homopiperidine rings and the side structures at the X position are important for manifestation of the proteasome inhibition activity of the RID-F derivatives, suggesting that further studies of this relationship are warranted.

3. Conclusion

Ridaifen-F (RID-F), a novel tamoxifen derivative, inhibited the human 20S proteasome. The structure–activity relationship of a series of RID-F derivatives revealed the fundamental structures required for proteasome inhibition. The derivatives inhibited the proteasome in cells, inducing apoptotic cell death. Based on kinetic analyses of the inhibition and docking simulation, we propose the inhibition mode of RID-Fs. Our next trial is underway to develop highly potent RID derivatives for *in vivo* use.

4. Experimental section

4.1. 20S proteasome fluorometric substrate assay

CT-L, PGPH, and T-L proteasome activities were determined by measuring the degradation rates of the fluorometric substrates succinyl-LLVY-AMC, Z-LLE-AMC, and Boc-LRR-AMC, respectively. Purified human 20S proteasomes (0.1 μg) were incubated with 50 μM (CT-L) or 20 μM (PGPH and T-L) fluorometric peptide substrate in the presence of varying concentrations of inhibitory compounds (0.01–10 μM) in 100 μL of assay buffer (25 mM HEPES, 0.5 mM EDTA, 0.03% SDS) at 37 °C. In the T-L activity assay, SDS was excluded from the assay buffer [47]. Reactions were monitored by AMC product formation (λ_{ex} = 380 nm, λ_{em} = 460 nm) for 1 h. The IC_{50}, defined as the compound concentration required for 50% inhibition of proteasome activity, was determined for each compound from the respective inhibition curve.

4.2. Growth inhibition assays

HEK293 cells (ER-negative) were cultured in Dulbecco's Modified Eagle Medium containing 10% fetal bovine serum, 100 units/mL of penicillin, and 0.1 mg/mL of streptomycin. HL-60 cells (ER-positive) were cultured in Iscove's Modified Dulbecco's Medium containing 10% fetal bovine serum, 100 units/mL of penicillin, and 0.1 mg/mL of streptomycin. Cells were seeded in duplicate wells in a 96-well plate

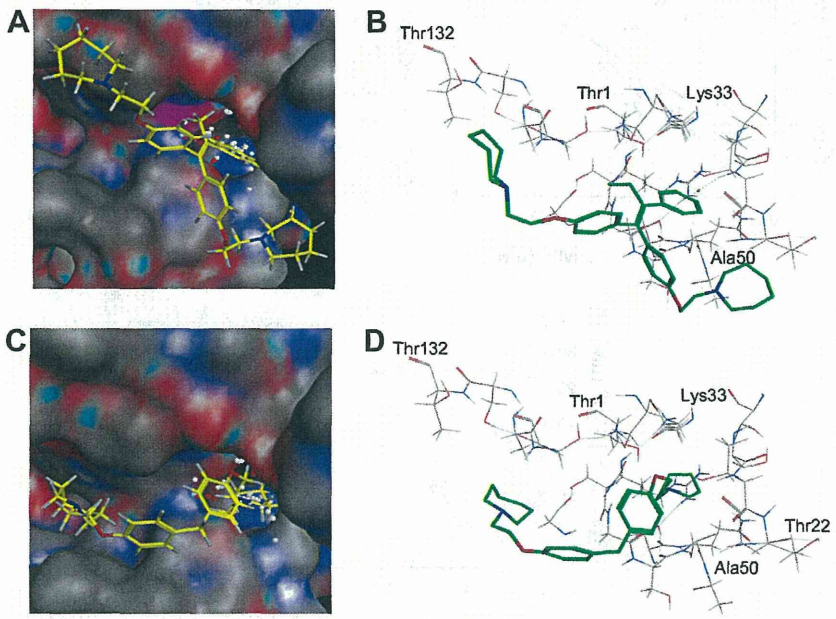

Fig. 6. Schematic view of RID-F (**6**) (panels A and B) or RID-F-S*4 (**25**) (panels C and D) – proteasome interactions. Images (panels A and C) represent the most likely binding modes. The binding pocket is shown as a solid surface with carbon atoms colored gray, N atoms colored blue, and O atoms colored red. Panels B and D show skeleton models of the binding modes.

at a density of 5×10^3 cells/well and were cultured for 48 h in medium alone or in medium containing an RID-F derivative at different concentrations (ranging from 0.1 to 20 μM). Cell viability and proliferation were evaluated by quantification of MTT reduction by mitochondrial dehydrogenases. Formazan dye production was measured by determining the 560/750 nm absorbance ratio after HCl/2-propanol extraction according to the manufacturer's protocol (Promega). The CyT_{50}, defined as the compound concentration required for 50% inhibition of cell proliferation, was determined for each compound from the respective inhibition curve.

4.3. Binding experiment

Purified human 20S proteasomes were incubated with varying concentrations of RID-F derivatives or the representative proteasome activity inhibitor MG132 for 1 h at 37 °C and then biotin-belactosin A was added at 1 μM. After an additional 1 h of incubation, proteins were separated by SDS-PAGE and transferred to a polyvinylidene difluoride (PVDF) membrane (Millipore). The membrane was blocked with 5% skim milk solution. Biotin-labeled proteins were visualized using streptavidin-HRP reagent and an ECL Plus membrane blot analysis detection kit (GE Healthcare).

4.4. Western blotting

HeLa cells (4×10^5 cells/well) were seeded in a 12-well plate and incubated with varying concentrations of RID-F derivatives for 24 h. The cells were then lysed with lysis buffer (62.5 mM Tris–HCl, 2% SDS, 10% glycerol, 0.1 mg/mL of phenylmethylsulfonyl fluoride, 10 μg/mL of leupeptin, 1 μg/mL of pepstatin A, and a phosphatase inhibitor cocktail (Nacalai Tesque Inc., Kyoto, Japan)). Equivalent amounts of protein (30 μg) were resolved by SDS-PAGE, transferred and immobilized onto PVDF membranes, and probed with primary and secondary antibodies. Anti-ubiquitin antibody (1:200 dilution; Santa Cruz Biotechnology), anti-actin antibody (1:10,000; Santa Cruz Biotechnology), and HRP-conjugated anti-mouse or anti-rabbit antibody (1:2000; Santa Cruz Biotechnology) were used. Immunodetection was performed as described above.

Apoptosis induced by RID-F derivatives was examined with HeLa cells. Cells (4×10^5 cells/well) were seeded in a 12-well plate and incubated with varying concentrations of RID-F derivatives for 24 h. Cleavage of PARP, which is a hallmark of apoptosis, was detected by Western blotting as described previously [48].

Conflict of interest

The authors declare no competing financial interest.

Acknowledgment

The authors thank Mie Tsuchida and Miho Hosoi for technical assistance and Dr. Tetuo Yoshida of Kyowa Hakko Kirin Co. for supplying belactosin A. The authors also thank Drs. Takao Yamori and Reiko Shinkura for helpful discussions. This study was supported by a Health Labour Sciences Research Grant from the Ministry of Health, Labour and Welfare, Japan to I.S. and a Grant-in-Aid for Scientific Research on Priority Area "Cancer" from the Ministry of Education, Culture, Sports, Science and Technology, Japan to T.M. M.S. received support from the Platform for Drug Discovery, Informatics, and Structural Life Science of the Ministry of Education, Culture, Sports, Science and Technology, Japan.

Abbreviations

AMC 7-amino-4-methylcoumarin
CT-L chymotrypsin-like
CyT_{50} half-maximum cytotoxicity concentration
4,4′-DHBP 4,4′-dihydroxybenzophenone
DMF dimethylformamide
ER estrogen receptor
IC_{50} half-maximum inhibitory concentration
HRP horseradish peroxidase
K_i inhibition constant
MTT (3-(4,5-dimethylthiazol-2-yl)-2,5-diphenyltetrazolium bromide
PARP poly-ADP ribose polymerase
PGPH peptidylglutamyl peptide hydrolase
p-TsOH *p*-toluenesulfonic acid
RID ridaifen
SDS sodium dodecyl sulfate
TAM tamoxifen
T-L trypsin-like
THF tetrahydrofuran.

Appendix A. Supplementary data

Supplementary data related to this article can be found at http://dx.doi.org/10.1016/j.ejmech.2013.11.009.

References

[1] A. Navon, A. Ciechanover, The 26S proteasome: from basic mechanisms to drug targeting, J. Biol. Chem. 284 (2009) 33713–33718.
[2] A.G. Eldridge, T. O'Brien, Therapeutic strategies within the ubiquitin proteasome system, Cell Death Differ. 17 (2010) 4–13.
[3] D. Hanahan, R.A. Weinberg, Hallmarks of cancer: the next generation, Cell 144 (2011) 646–674.
[4] M.A. Shahshahan, M.N. Beckley, A.R. Jazirehi, Potential usage of proteasome inhibitor bortezomib (Velcade, PS-341) in the treatment of metastatic melanoma: basic and clinical aspects, Am. J. Cancer Res. 1 (2011) 913–924.
[5] M.A. Gräwert, M. Groll, Exploiting nature's rich source of proteasome inhibitors as starting points in drug development, Chem. Commun. (Camb.) 48 (2012) 1364–1378.
[6] P. Lawasut, D. Chauhan, J. Laubach, C. Hayes, C. Fabre, M. Maglio, C. Mitsiades, T. Hideshima, K.C. Anderson, P.G. Richardson, New proteasome inhibitors in myeloma, Curr. Hematol. Malig. Rep. 7 (2012) 258–266.
[7] A. Mullard, Next-generation proteasome blockers promise safer cancer therapy, Nat. Med. 18 (2012) 7.
[8] A. Katsnelson, Next-generation proteasome inhibitor approved in multiple myeloma, Nat. Biotechnol. (2012) 1011–1012.
[9] A.A. Argyriou, G. Iconomou, H.P. Kalofonos, Bortezomib-induced peripheral neuropathy in multiple myeloma: a comprehensive review of the literature, Blood 112 (2008) 1593–1599.
[10] L. Meng, R. Mohan, B.H. Kwok, M. Elofsson, N. Sin, C.M. Crews, Epoxomicin, a potent and selective proteasome inhibitor, exhibits in vivo anti-inflammatory activity, Proc. Natl. Acad. Sci. U. S. A. 96 (1999) 10403–10408.
[11] J. Myung, K.B. Kim, K. Lindsten, N.P. Dantuma, C.M. Crws, Lack of proteasome active site allostery as revealed by subunit-specific inhibitors, Mol. Cell 7 (2001) 411–420.
[12] D.J. Kuhn, Q. Chen, P.M. Voorhees, J.S. Strader, K.D. Shenk, C.M. Sun, S.D. Demo, M.K. Bennett, F.W. van Leeuwen, A.A. Chanan-Khan, R.Z. Orlowski, Potent activity of carfilzomib, a novel, irreversible inhibitor of the ubiquitin-proteasome pathway, against preclinical models of multiple myeloma, Blood 110 (2007) 3281–3290.
[13] D. Chen, M. Frezza, S. Schmitt, J. Kanwar, Q.P. Dou, Bortezomib as the first proteasome inhibitor anticancer drug: current status and future perspectives, Curr. Cancer Drug Targets 11 (2011) 239–253.
[14] E. Genin, M. Reboud-Ravaux, J. Vidal, Proteasome inhibitors: recent advances and new perspectives in medicinal chemistry, Curr. Top Med. Chem. 10 (2010) 232–256.
[15] G. Schmidtke, H.G. Holzhutter, M. Bogyo, N. Kairies, M. Groll, R. de Giuli, S. Emch, M. Groettrup, How an inhibitor of the HIV-I protease modulates proteasome activity, J. Biol. Chem. 274 (1999) 35734–35740.
[16] P. Furet, P. Imbach, P. Fuerst, M. Lang, M. Noorani, J. Zimmermann, C. Garcia-Echeverria, Structure-based optimisation of 2-aminobenzylstatine derivatives: potent and selective inhibitors of the chymotrypsin-like activity of the human 20S proteasome, Bioorg. Med. Chem. Lett. 12 (2002) 1331–1334.
[17] P. Furet, P. Imbach, M. Noorani, J. Koeppler, K. Laumen, M. Lang, V. Guagnano, P. Fuerst, J. Roesel, J. Zimmermann, C. Garcia-Echeverria, Entry into a new class of potent proteasome inhibitors having high antiproliferative activity by structure-based design, J. Med. Chem. 47 (2004) 4810–4813.

[18] R.T. Lum, M.G. Nelson, A. Joly, A.G. Horsma, G. Lee, S.M. Meyer, M.M. Wick, S.R. Schow, Selective inhibition of the chymotrypsin-like activity of the 20S proteasome by 5-methoxy-1-indanone dipeptide benzamides, Bioorg. Med. Chem. Lett. 8 (1998) 209–214.
[19] N. Basse, D. Papapostolou, M. Pagano, M. Reboud-Ravaux, E. Bernard, A.S. Felten, R. Vanderesse, Development of lipopeptides for inhibiting 20S proteasomes, Bioorg. Med. Chem. Lett. 16 (2006) 3277–3281.
[20] C. Blackburn, K.M. Gigstad, P. Hales, K. Garcia, M. Jones, F.J. Bruzzese, C. Barrett, J.X. Liu, T.A. Soucy, D.S. Sappal, N. Bump, E.J. Olhava, P. Fleming, L.R. Dick, C. Tsu, M.D. Sintchak, J.L. Blank, Characterization of a new series of non-covalent proteasome inhibitors with exquisite potency and selectivity for the 20S β5-subunit, Biochem. J. 430 (2010) 461–476.
[21] G. Lin, T. Chidawanyika, C. Tsu, T. Warrier, J. Vaubourgeix, C. Blackburn, K. Gigstad, M. Sintchak, L. Dick, C. Nathan, N,C-Capped dipeptides with selectivity for mycobacterial proteasome over human proteasomes: role of S3 and S1 binding pockets, J. Am. Chem. Soc. 135 (2013) 9968–9971.
[22] Y. Koguchi, J. Kohno, M. Nishio, K. Takahashi, T. Okuda, T. Ohnuki, S. Komatsubara, TMC-95A, B, C, and D, novel proteasome inhibitors produced by *Apiospora montagnei Sacc.* TC 1093. Taxonomy, production, isolation, and biological activities, J. Antibiot. (Tokyo) 53 (2000) 105–109.
[23] M. Groll, R. Huber, L. Moroder, The persisting challenge of selective and specific proteasome inhibition, J. Pept. Sci. 15 (2009) 58–66.
[24] N. Basse, S. Piguel, D. Papapostolou, A. Ferrier-Berthelot, N. Richy, M. Pagano, P. Sarthou, J. Sobczak-Thépot, M. Reboud-Ravaux, J. Vidal, Linear TMC-95-based proteasome inhibitors, J. Med. Chem. 50 (2007) 2842–2850.
[25] A. Desvergne, E. Genin, X. Maréchal, N. Gallastegui, L. Dufau, N. Richy, M. Groll, J. Vidal, M. Reboud-Ravaux, Dimerized linear mimics of a natural cyclopeptide (TMC-95A) are potent noncovalent inhibitors of the eukaryotic 20S proteasome, J. Med. Chem. 56 (2013) 3367–3378.
[26] N. Basse, M. Montes, X. Marechal, L. Qin, M. Bouvier-Durand, E. Genin, J. Vidal, B.O. Villoutreix, M. Reboud-Ravaux, Novel organic proteasome inhibitors identified by virtual and *in vitro* screening, J. Med. Chem. 53 (2010) 509–513.
[27] S. Mandlekar, A.N. Kong, Mechanisms of tamoxifen-induced apoptosis, Apoptosis 6 (2001) 469–477.
[28] C. Ferlini, G. Scambia, M. Marone, M. Distefano, C. Gaggini, G. Ferrandina, A. Fattorossi, G. Isola, P. Benedetti Panici, S. Mancuso, Tamoxifen induces oxidative stress and apoptosis in oestrogen receptor-negative human cancer cell lines, Br. J. Cancer 79 (1999) 257–263.
[29] Y. Kang, R. Cortina, R.R. Perry, Role of c-myc in tamoxifen-induced apoptosis estrogen-independent breast cancer cells, J. Natl. Cancer Inst. 88 (1996) 279–284.
[30] Y. Nagahara, I. Shiina, K. Nakata, A. Sasaki, T. Miyamoto, M. Ikekita, Induction of mitochondria-involved apoptosis in estrogen receptor-negative cells by a novel tamoxifen derivative, ridaifen-B, Cancer Sci. 99 (2008) 608–614.
[31] I. Shiina, Y. Sano, K. Nakata, T. Kikuchi, A. Sasaki, M. Ikekita, Y. Nagahara, Y. Hasome, T. Yamori, K. Yamazaki, Synthesis and pharmacological evaluation of the novel pseudo-symmetrical tamoxifen derivatives as anti-tumor agents, Biochem. Pharmacol. 75 (2008) 1014–1026.
[32] I. Shiina, Y. Sano, K. Nakata, M. Suzuki, T. Yokoyama, A. Sasaki, T. Orikasa, T. Miyamoto, M. Ikekita, Y. Nagahara, Y. Hasome, An expeditious synthesis of tamoxifen, a representative SERM (selective estrogen receptor modulator), via the three-component coupling reaction among aromatic aldehyde, cinnamyltrimethylsilane, and β-chlorophenetole, Bioorg. Med. Chem. 15 (2007) 7599–7617.
[33] I. Shiina, Y. Sano, K. Nakata, T. Kikuchi, A. Sasaki, M. Ikekita, Y. Hasome, Synthesis of the new pseudo-symmetrical tamoxifen derivatives and their anti-tumor activity, Bioorg. Med. Chem. Lett. 17 (2007) 2421–2424.
[34] I. Shiina, M. Ikekita, T. Matsunaga, Y. Nagahara, Anticancer agent containing tamoxifen analogue as active ingredient, Jpn. Kokai Tokkyo Koho (11 May 2006). JP2006117648.
[35] I. Shiina, Proteasome inhibitor which contains tamoxifen analogue as an active ingredient, Jpn. Kokai Tokkyo Koho (24 April 2008). JP2008094836.
[36] T. Mukaiyama, Titanium tetrachloride in organic synthesis, Angew. Chem. Int. Ed. 16 (1977) 817–826.
[37] D.D. Yu, B.M. Forman, Simple and efficient production of (*Z*)-4-hydroxytamoxifen, a potent estrogen receptor modulator, J. Org. Chem. 68 (2003) 9489–9491.
[38] M.L. Connolly, The molecular surface package, J. Mol. Graphics 11 (1993) 139–141.
[39] M. Hendlich, F. Rippmann, G. Barnickel, LIGSITE: automatic and efficient detection of potential small molecule-binding sites in proteins, J. Mol. Graph. Model. 15 (1997) 359–363.
[40] T.D. Penning, N.S. Chandrakumar, B.B. Chen, H.Y. Chen, B.N. Desai, S.W. Djuric, S.H. Docter, A.F. Gasiecki, R.A. Haack, J.M. Miyashiro, M.A. Russell, S.S. Yu, D.G. Corley, R.C. Durley, B.F. Kilpatrick, B.L. Parnas, L.J. Askonas, J.K. Gierse, E.I. Harding, M.K. Highkin, J.F. Kachur, S.H. Kim, G.G. Krivi, D. Villani-Price, E.Y. Pyla, W.G. Smith, N.S. Ghoreishi-Haack, Structure–activity relationship studies on 1-[2-(4-phenylphenoxy)ethyl]pyrrolidine (SC-22716), a potent inhibitor of leukotriene A_4 (LTA_4) hydrolase, J. Med. Chem. 43 (2000) 721–735.
[41] M. Hasegawa, K. Kinoshita, C. Nishimura, U. Matsumura, M. Shionyu, S. Ikeda, T. Mizukami, Affinity labeling of the proteasome by a belactosin A derived inhibitor, Bioorg. Med. Chem. Lett. 18 (2008) 5668–5671.
[42] W. Heinemeyer, J.A. Kleinschmidt, J. Saidowsky, C. Escher, D.H. Wolf, Proteinase yscE, the yeast proteasome/multicatalytic-multifunctional proteinase: mutants unravel its function in stress induced proteolysis and uncover its necessity for cell survival, EMBO J. 10 (1991) 555–562.
[43] R. Gueckel, C. Enenkel, D.H. Wolf, W. Hilt, Mutations in the yeast proteasome beta-type subunit Pre3 uncover position-dependent effects on proteasomal peptidase activity and *in vivo* function, J. Biol. Chem. 273 (1998) 19443–19452.
[44] M. Groll, L. Ditzel, J. Löwe, D. Stock, M. Bochtler, H.D. Bartunik, R. Huber, Structure of 20S proteasome from yeast at 2.4 Å resolution, Nature 386 (1997) 463–471.
[45] M. Unno, T. Mizushima, Y. Morimoto, Y. Tomisugi, K. Tanaka, N. Yasuoka, T. Tsukihara, The structure of the mammalian 20S proteasome at 2.75 Å resolution, Structure 10 (2002) 609–618.
[46] J. Goto, R. Kataoka, H. Muta, N. Hirayama, ASEDock-docking based on alpha spheres and excluded volumes, J. Chem. Inf. Model. 48 (2008) 583–590.
[47] K. Tanaka, T. Yoshimura, A. Ichihara, Role of substrate in reversible activation of proteasomes (multi-protease complexes) by sodium dodecyl sulfate, J. Biochem. (Tokyo) 106 (1989) 495–500.
[48] T. Kunoh, T. Noda, K. Koseki, M. Sekigawa, M. Takagi, K. Shin-ya, N. Goshima, S. Iemura, T. Natsume, S. Wada, Y. Mukai, S. Ohta, R. Sasaki, T. Mizukami, A novel human dynactin-associated protein, dynAP, promotes activation of Akt, and ergosterol-related compounds induce dynAP-dependent apoptosis of human cancer cells, Mol. Cancer Ther. 9 (2010) 2934–2942.